Bioinspired Electro-Thermo-Hygro Reversible Shape-Changing Materials by 4D Printing

A. Le Duigou[a*], G. Chabaud[a], F. Scarpa[b], M. Castro[a]

[a] Polymer and Composites, Univ.Bretagne Sud, UMR CNRS 6027, IRDL, F-56100 Lorient, France

[b] Bristol Composites Institute (ACCIS), University of Bristol, BS8 1TR Bristol, UK

*Corresponding author: antoine.le-duigou@univ-ubs.fr

Abstract

Hygromorph composites are moisture-induced shape changing materials that are increasingly studied to develop autonomously actuated deployable structures. The morphing mechanism is based on the high affinity for moisture and the hygro-expansive nature of at least one component, combined with a bilayer microstructure. Among available hygromorphs those consisting in cellulosic or hydrogel material-based actuators trigger fast responses to moisture. Their stiffness however decreases significantly with the moisture content and that restricts their potential application as soft actuators.

This work proposes a novel 4D printed multi-stimuli-responsive structural material based on conductive carbon reinforcements and combined with a moisture sensitive polymer. These 4D printed materials possess a microstructure that provides the capability of natural actuators like pine cones. The actuation of these functional materials could be either triggered passively by the variation of the ambient moisture, or by electro-heating, with the latter leading to the control of the moisture content in initially wet samples via Joule effects. This new class of functional materials shows an increase of the actuation speed by a factor 10 compared to other existing hygromorphs with the same responsiveness. When the electrical heating is turned off, passive cooling and moisture driven actuation is triggered in a full reversible mode.

Keywords: Hygromorph, Fused filament fabrication, 4D printing, morphing, moisture, electro-active

1. Introduction

Additive manufacturing with 4D printing combines 3D printing techniques and the use of materials with time-dependent properties when an external stimulus is present [1–3]. 4D printing allows an easier manufacturing of smart materials with embedded functionalities thanks to the capability of creating complex architectures and the design of pre-programmed structures [4]. Two types of stimulus-responsive materials currently exist: shape-changing materials with spontaneous response to stimuli ,and shape memory materials that return to their shape after the external actuation [5,6] .

Environmentally-driven actuation mechanisms are currently attracting some significant interest to design autonomous deploying systems for which low maintenance, cost and low energy consumptions are paramount. Current efforts in the 4D printing community are mainly dedicated to exploit the use of thermally activated polymers or related composites [7]. Recent research activities have however been focused on the use of electrical actuation to improve the control of the temperature gradient, in particular for continuous carbon fibre 4D printed composites. Yang *et al.* have evaluated carbon fibre/polyether-ether-ketone (PEEK) and polylactic acid (PLA) composites with the thermal actuation triggered by electro-heating [8]. Real environmental and atmospheric conditions are however more complex, and changes of temperature are always coupled with variations of humidity. The moisture-induced actuation of additive manufacturing materials is rarely discussed aside from cases related to the self-folding hydrogel-based micro-actuators [9–11] or 2 GPa stiff polymer/acrylated monomers hydrogel systems [12]. In recent time natural fibre hygromorph wood/PLA biocomposites [13,14] with high actuation stiffness and strength have been developed for structural up-scaled applications, in particular for buildings (cladding/façade, shading systems and solar tracker). Hygromorph composites are however relatively slow velocity actuators, limited by the moisture transport kinetics that could constitute a real bottleneck in technical applications where actuation control and faster responses are required. Unlike thermally-activated polymers based on the presence of one stimulus, hygromorphs are hygroscopically activated, and they are therefore also temperature dependent. Few studies have however been carried out on materials that exploit the hygro-expansive properties of conductive paper or hydrogels with an electricity-driven actuation [15–19]. In the cited references, the response was manually controlled by

electro-heating to trigger a faster deployment rate. Dual actuators have also been activated by using UV radiation and moisture variation with laser printed toner-coated paper/biaxially oriented polypropylene actuators [20] and on graphene oxide (GO) / biaxially oriented polypropylene (BOPP) systems [21]. Those materials allowed to reach high curvature deformations (1 cm^{-1}) with a short actuation time (≈ 10-20s) due to their low stiffness. Their applications have been therefore limited to small scale prototypes and their utilization to non-harsh environments. Mao et al. [22] have also developed a shape memory polymer (SMP) "Grey60"/ Elastomer "Tangoblack" or "Verowhite"/ Hydrogel actuator that enables to combine moisture and temperature to trigger actuation while providing a higher level of stiffness for the material system. The hygroscopic actuation of the hydrogel was influenced by the evolution of the stiffness of the SMP with the temperature. The overall actuation of this hydrogel/SMP system is however not completely controllable and the reactivity is still rather low (10-20 hours for a full actuation cycle).

With the present work we present a novel concept of 4D printed multi-stimuli-responsive structural material based on the electro-thermal activation of hygromorph composites. Continuous carbon fibres (cCF) along with a moisture sensitive polyamide matrix (PA6) are used here with a specific microstructure that biomimics at microscale natural hydraulic actuators like pine cones. We have first printed Polyamide 6-I coated continuous carbon fibres/Polyamide 6 bilayers (cCF:PA6-I/PA6). PA6-I shows a higher glass transition temperature (Tg) than PA6, *i.e.* 123°C and 41°C respectively (evaluated by DSC measurements, not shown here). Then, samples have been stored at different relative humidity levels (9%, 33%, 50%, 75% and 98%) and at room temperature (23°C) to evaluate their autonomous hygromorphic behaviour in term of curvature. Similar composite materials have been prepared then as platforms for electro-thermo-hygromorphs and their actuation mechanism evaluated at different voltages (10V and 15V) onto saturated samples at 98% RH and 23°C. We have finally analysed the influence of the electrical stimulus on the heating of the material, the moisture content and the speed of curvature as well as on the amplitude of the curvature induced by the multiphysics actuation.

2. Results and discussion

2.1 Concept of 4D printed electro-thermo-hygromorph structural composite materials

Polyamide and carbon fibres have been selected as components to design this smart composite material. Current 4D printed smart composites for actuation are mainly based on the coefficient of thermal expansion (CTE) of the polymer (α) that drives the responsiveness and reactivity of the actuator. We use here well-known moisture-sensitive polymers such as Polyamide (PA6 and PA6-I). The CTE of the polymers along the longitudinal and transverse directions are however 3800 and 5000 times lower than hygroscopic expansion (β) (see Table 1). This implies that the thermal strain induced by a variation in temperature would be significantly lower than the hygroscopic strain induced by the variation of humidity. There is therefore potential to use the moisture and the hygroscopicity of the material as a driver for the actuation. The direction of the carbon fibres also affects the thermal and the hygroscopic expansions (Table 1). Although along the fibres longitudinal direction the hygroscopic and thermal expansions are negligible, the α and β coefficients of the composites along the transverse direction assume the highest strain expansion potentials due to the anisotropy of the carbon fibres [23]. The orientation of the fibres is therefore a critical parameter to design the microstructure of shape-changing composite materials made with thermally and/or hygroscopically active and passive phases.

Table 1: Values of coefficients of thermal and hygroscopic expansion for cCF:PA6-I longitudinal, transverse and for pure PA6.

Materials	**α (10^{-6} . K^{-1})**	**β (-)**
cCF:PA6-I Longitudinal	-	-
cCF:PA6-I Transverse	49 ± 4	0.26 ± 0.03
PA6	90 [24]	0.34 ± 0.04

Continuous fibre composite materials and a 4D printing process were selected to control the orientation of the fibres and consequently their stiffness, thermal and the hygroscopic anisotropy properties that are key factors to promote the bending actuation.

The hygromorph composite materials possess a bilayer microstructure inspired by the one of natural hydraulic actuators (pine cones for instance [25][26]), printed with two layers having different hygro-mechanical properties. The layer made with the continuous carbon fibres embedded in a PA6-I matrix is hygroscopically and thermally passive (*i.e.*, with a low thermo-hygro expansion) but electrically

active. The printed cCF:PA6-I layer is used here as a mechanically resistant lamina with high durable stiffness against moisture, while having at the same time fibres that act as an electrical circuit. The other layer of pure PA6 matrix (Figure 1a) is the hygroscopically and thermally active one. The optimal stacking sequence for a maximal bending actuation is determined via bimetallic strip theory calculations [27] (equation 1). The model is based on the thickness ratio between active and passive layers and their hygro-elastic properties [28]. An optimized stacking sequence has been used to induce a large displacement of hygromorph materials [23]. An increase of the thickness would geometrically increase the bending stiffness and the actuation force but would lower targeted morphing. Hence, depending on the requirements and the application, compromise shall be found between the stiffness and the actuation's responsiveness. The differential hygroscopic expansion between layers leads to the bending actuation of the hygromorph composite in various external humid environments (from 10 to 95% RH) (Figure 1a). An autonomous response with large responsiveness is produced (0.088 ± 0.011), however a slow response was also noticed due to the transitory and diffusive water transport within the material [29,30]. This may limit the up-scaling of hygromorph composites structures, and also limit their use for applications like soft robotics, for which passive actuation is less of a requirement than controlled actuation.

To overcome this issue, we have devised a mechanism to actively control the moisture content and the resulting hygroscopic strains and therefore reaching a dedicated position of the shape-changing composite material. The concept is based on the work of Hamedi *et al.* [15], who exploited the hygroscopic expansion in an electrically activated paper. We use here a similar approach to develop electro-thermo-hygromorphs through 4D printing for structural and load-bearing composite materials, rather than in soft solids like paper. The electrical functionality is here embedded within the cCF:PA6-I/PA6 hygromorph composites with the carbon fibres both playing the role of the reinforcement and the electrically conductive path. The adjustment of the pattern of the printed carbon fibres makes it possible to control the stiffness distribution along the sample, *i.e.* its responsiveness and electrical conductivity, and thus finally the reactivity. Fused Filament Fabrication (FFF) has been used here to construct the architecture of the electrical circuit and the reinforcement. The layer containing the continuous carbon

fibres is printed in a pre-optimized U-shape pattern to promote the electrical conductivity while maintaining a degree of freedom for the structure to actuate.

The application of an electrical field to the moisture saturated sample (RH=98% in Figure 1b) leads to an electrical Joule effect-induced heating and a rise of the temperature that may vary versus the input voltage and the electrical conductivity of the composite layer. The variation of the temperature also leads to a change of the moisture content. The increase in temperature, potentially combined with the thermal expansion of the polymeric material would contribute to a thermal actuation similarly observed by Wang et al. [31].

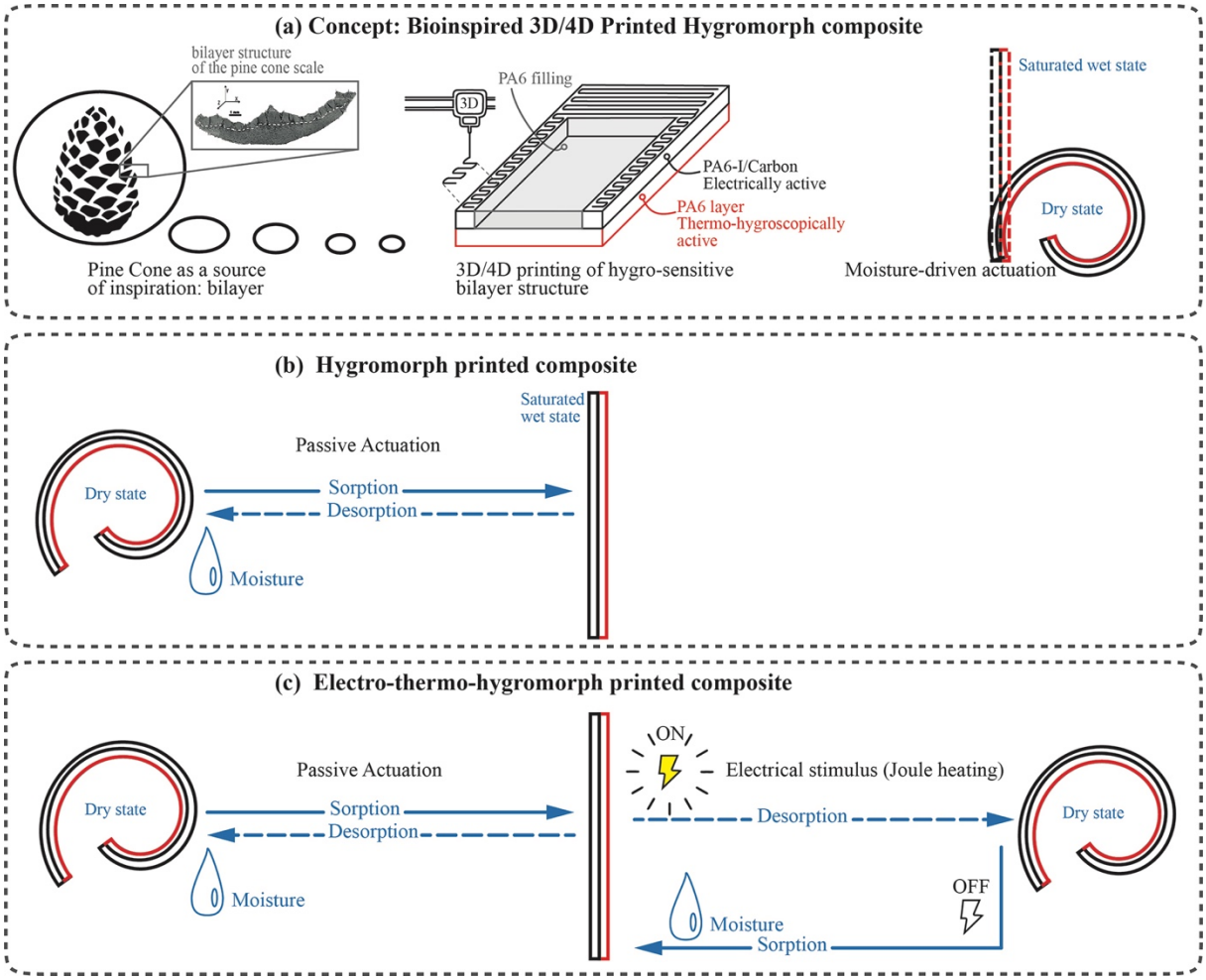

Figure 1: (a) Principle of hygromorph composite materials. A pine cone actuator microstructure (inset: bilayer structure of the pine cone scale, adapted from [25]) is mimicked in a bilayer configuration. The materials are selected with at least one of them being moisture sensitive (the PA6 polymer in this case). 3D printing enables the manufacturing of complex architecture possessing various stiffness and electrical conductivity distributions. The variation of the relative humidity leads to moisture uptake and internal hygroscopic stresses distributions within the bilayer and a resulting bending actuation. (b) Initial state of the bilayer composite dried at 9% RH and 23°C, *i.e.* the composite is curved. Upon moisture sorption, the composite straightens. (c) From dry to wet state the composite is similar to (b) in shape. At saturated wet state, an electrical stimulus leads to an increase of temperature by Joule effect. The moisture content then quickly reduces and allows to control the actuation (return to dry curved state). When the electrical current is switched-off the temperature decreases and the moisture content increases, depending on the environmental RH at which the sample is exposed to. The material behaves as an autonomous and reversible hygromorph actuator.

Contrary to the water diffusion within a polymer or a composite, the thermal diffusion induced by the electro-heating effect is a fast kinetics phenomenon [8]. Moisture-driven actuation could be therefore accelerated through the desorption of the moisture out of the composite material. The stiffness and the hygroscopic shrinkage of each layer is altered by the presence of this mechanism. Once the electrical field is switched-off, the autonomous moisture sorption drives back the morphing behaviour. In the present concept, the hygroscopic behaviour of the bilayer is used for actuation responsiveness, while the electrical stimulus allows to trig and enhance the speed of the actuation.

2.2 cCF:PA6-I/PA6 bilayers as hygromorph actuators

Continuous carbon fibre reinforced polyamide based composites have been manufactured with a rectangular shape (L = 70 mm and w = 20 mm) based on an optimal bilayer architecture designed using an equivalent bimetallic beam model (equation 1). The cCF:PA6-I layer has an overall thickness of 0.125 mm and is printed transversally to the length of the sample. The conductive network (not triggered during this step) has a rectangular-type U-shape pattern (Figure 2a) with a L/W ratio of 0.25. The ratio has been selected from previous trials due to its higher responsiveness (see supplementary information Table S1). When exposed to various humid environments (0, 9, 33, 50, 75, 98% RH) the cCF:PA6-I/PA6 bilayers show a very pronounced actuation authority (Figure 2a). Dried samples exhibit a high curvature value at low RH values, then straighten in a humid environment. From image analysis it is possible to measure the relative curvature ΔK, which is the difference between the initial curvature $K_{initial}$ and the final one K_t. The actuated curvature evolves non-linearly with the sorption time. A quick reactivity is observed during the initial time of sorption and once the saturation is reached the relative curvature has its maximum. A maximum relative curvature of 0.088 ± 0.011 mm^{-1} (Figure 2b) is recorded for samples stored at 98% RH and 23°C; this value is comparable to the one exhibited by natural fibres, paper or hydrogel based hygromorph materials with similar thickness [32–34]. The maximum curvature depends on the moisture content (Figure 2b and c). The higher the content, the larger the actuation responsiveness (Figure 2b). The reactivity however appears not to be affected by the moisture content, and circa 12 hours have been necessary for the full and autonomous actuation of

the cCF:PA6-I/PA6 bilayers. This timeline corresponds to the moisture sorption, diffusion and complete saturation within the material itself.

After reaching a stable value of the curvature at 98%RH, the cCF:PA6-I/PA6 bilayers are placed in a dry environment (RH = 9%) at room temperature (T = 23°C). During the drying step, the final value of ΔK is reached even faster (350 mins) than in the case of sorption (1000 mins – see Figure 2c). Compared to the initial weight of the sample stabilized at 9% RH, a close value is observed meaning a reversible moisture transport (Figure 2d). The faster reach of the ΔK value also clearly shows that the mechanisms associated to the moisture transport and the autonomous responsiveness are fully reversible, however the reactivity is different between sorption and desorption phases. This actuation asymmetry has also been observed on natural fibre based hygromorph actuators where the active and the passive layers are based on similar materials [13,15]. The hygro-mechanical effects within the passive layer are however different if sorption or desorption are occurring. During sorption, the bilayers tend to straighten and the passive layer (cCF:PA6-I) is transversally loaded in compressive mode. On the contrary, during desorption the bilayers tend to bend and the passive layer is transversally loaded in tension. As the transverse compressive stiffness of unidirectional laminates is in general higher than the transverse tensile one [35], the passive layer results to be easier to bend than to straighten, and this will affect the speed of the actuation.

The global hygromorph behaviour (sorption/desorption) is illustrated by the evolution of the relative curvature versus the moisture content for several moist and desorption conditions (from 98% RH to 9% RH - Figure 2.e). The relative curvature shows almost linear trends for what it concerns the moisture content over the sorption/desorption processes (R^2= 0.99 for sorption step and R^2=0. 98 for desorption step). The slopes of the curves are also almost identical in magnitude (0.011 for sorption and 0.010 for desorption), and that indicates that the same mechanisms are very likely to be involved in the two processes. The amplitude of the radius of curvature generated by the actuation of the hygromorph composite materials can be therefore predicted by tracking the relative humidity. This feature also suggests that these smart materials could also be used as moisture sensors.

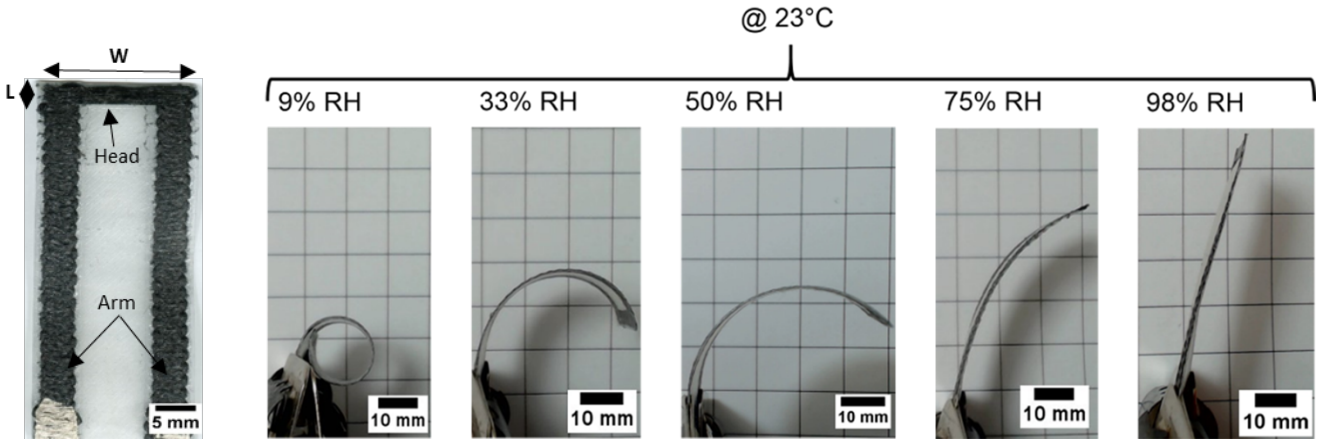
W
L
Head
Arm
5 mm
@ 23°C
9% RH
33% RH
50% RH
75% RH
98% RH
10 mm
10 mm
10 mm
10 mm
10 mm

(a)

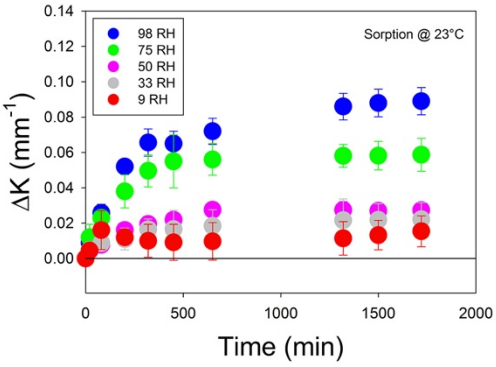
98 RH
75 RH
50 RH
33 RH
9 RH
Sorption @ 23°C
ΔK (mm-1)
Time (min)

(b)

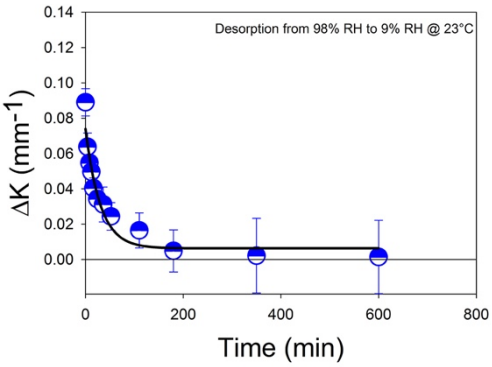
Desorption from 98% RH to 9% RH @ 23°C
ΔK (mm-1)
Time (min)

(c)

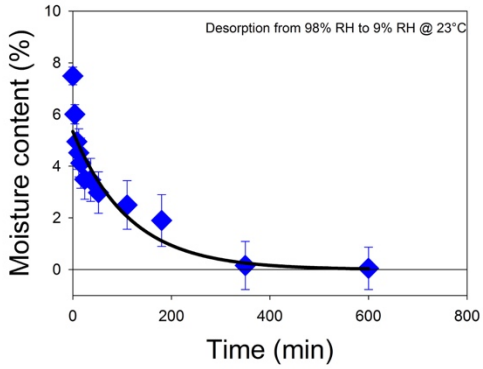
Desorption from 98% RH to 9% RH @ 23°C
Moisture content (%)
Time (min)

(d)

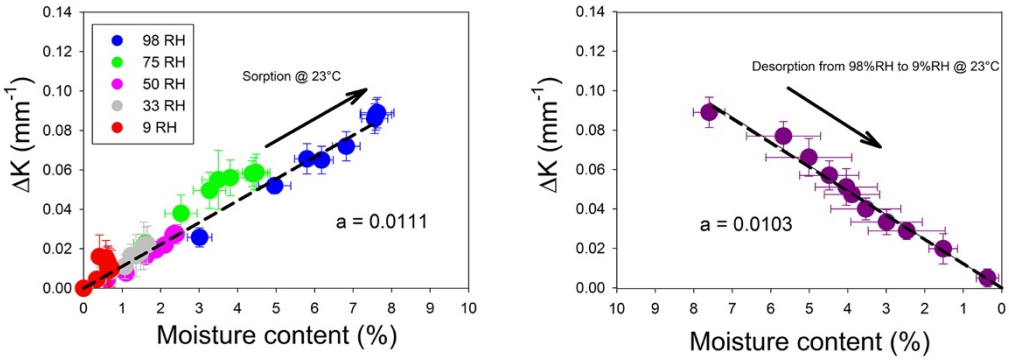
98 RH
75 RH
50 RH
33 RH
9 RH
Sorption @ 23°C
a = 0.0111
ΔK (mm-1)
Moisture content (%)
Desorption from 98%RH to 9%RH @ 23°C
a = 0.0103
ΔK (mm-1)
Moisture content (%)

(e)

Figure 2 (a) Bilayer cCF:PA6-I/PA6 U-shape sample with transverse printed pattern and its shape evolution when the relative humidity is increased from dry (9% RH) to a wet environment (98% RH) at 23°C. (b) The evolution of the relative curvature actuation for different humidity levels shows the increase in actuation reactivity and responsiveness with the moisture content during sorption. (c) The evolution of the relative curvature of the printed cCF:PA6-I during passive desorption from 98% RH to 9% RH (exponential decay fit of $R^2 = 0.960$) at 23°C shows the reversibility of the actuation (d) Evolution of the moisture content during desorption from 98% RH to 9% RH fitted with an exponential decay fit ($R^2 = 0.884$). (e) Evolution of the relative curvature ΔK over a variation of moisture content during sorption at several RH levels (left) and desorption from 98% RH to 9%RH (right) at 23°C. The changes of curvature due to sorption and desorption versus the moisture show a linear behaviour (R^2= 0.99 for sorption and R^2=0.98 for desorption) that allows to track the maximum amplitude of the induced curvature knowing the moisture content.

2.3 cCF:PA6-I/PA6 bilayers as electro-thermo-hygromorph actuators

Printed cCF:PA6-I composites are used here as a load-bearing layer with an electrical circuit. The multifunctional composite material provides a passive moisture-induced morphing shape capability and an active electrically-controlled phase. Two input voltages (10 and 15V) are applied thanks to the U-shaped printed pattern to control the moisture content. Those voltages are chosen to use a low input electric power (0.1W and 0.6W for 10 and 15V, respectively), and they are also compatible with analogous values for soft actuators reported in open literature [15–17].

Electro-heating leads to a heterogeneous temperature field within 120 seconds (Figure 3a). With an input of 15V, the cCF:PA6-I area reaches an average temperature of 40.0 ± 1.8°C. A similar but less pronounced behaviour is observed at the lower applied voltage of 10V, with an average temperature of 29.2 ± 1.3°C. (Figure 3b). The current circulates through the shortest pathway and prevents in this case the formation of a homogeneous heating field. Furthermore, at the end of one of the arms near the head zone an unusual temperature peak of 65°C has been observed for the five replicates (yellow spot in Figure 3a). This high value of local temperature is due to printing-induced defects which cause a weak contact and therefore a high resistance between one arm and the head. This point will be further discussed. Those high values of temperature can lead to temperature-induced damages (Figure 3.c). The zone of pure PA6 in the middle of the U-shape layer is hardly affected by the electro-heating, and this restrains to the area where the carbon fibres are located the surface for the electro-actuation. In our work we have used a commercial printer to make the case for the feasibility study, however printing parameters such as the fibre trajectory have not been fully customized.

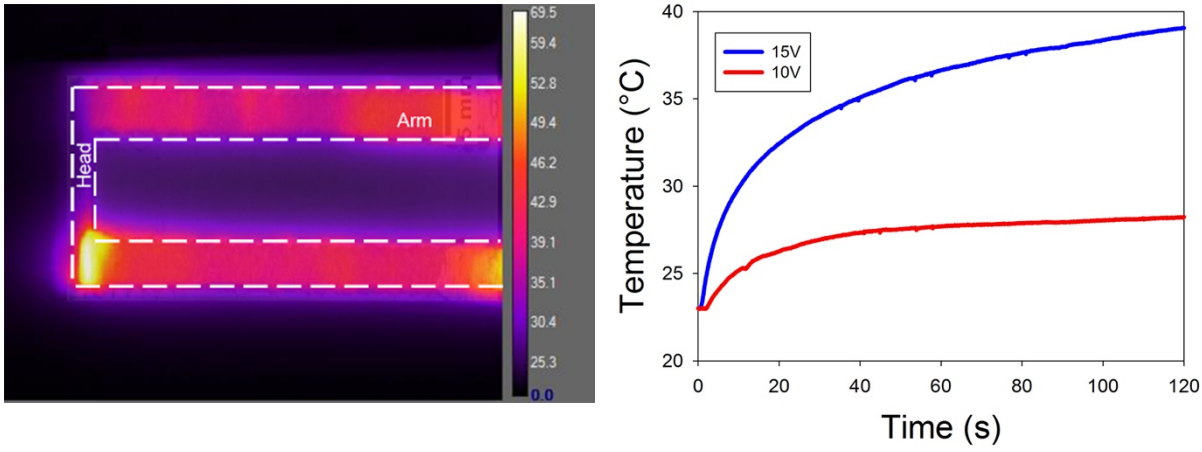

(a) (b)

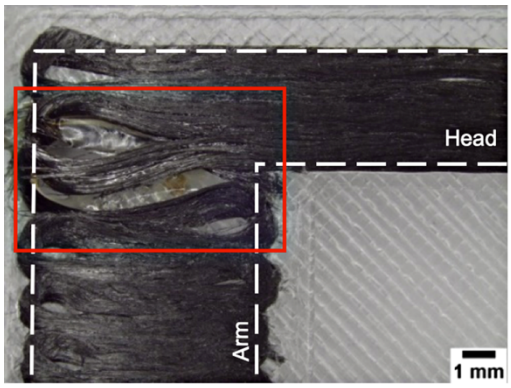

(c)

Figure 3: (a) Infrared thermography image of the hygromorph material with the printed electric circuit at steady state and 15V. The image shows the heterogeneity of the heating linked with printing defects. (b) Evolution of the average temperature in the arm and in the head of the cCF:PA6-I layers at 10V and 15V. (c) Example of a damage related to hot spot that is induced by the printing process (affecting the electrical conductivity of the sample).

The cCF:PA6-I/PA6 bilayers printed with this pattern nevertheless feature peak temperatures lower than those measured by Amjadi *et al.* [16] (around 70°C) and Hamedi *et al.* [15] (around 80-100°C) on thin electro-active papers. The electro-heating of these hygromorph composite materials did not cause to overcome the glass transition temperature (T_g) of the PA6 (50°C) of the thermally active layer, nor the one of the PA6-I (135°C) belonging to the cCF:PA6-I layer [23]. Low chain mobility, low free volume variation of the glassy polymer and therefore a low thermal expansion is observed when a polymer is close or crosses the T_g [36]. During the first actuation step thermal strains are very small, and therefore the contribution of a thermally-induced actuation is negligible. The elastic properties of the composite laminates do evolve with temperature, but only significantly above 60°C for the transverse cCF:PA6-I, and beyond 80°C for the longitudinally printed cCF:PA6-I patterns (see supplementary information).

Therefore, during the electrical stimulus, the elastic properties of the composite could be considered as constant.

The moisture content within the hygromorph materials after the electrical stimulus and the increase of temperature has been quantified with reference to an initial wet state of 98% RH. The moisture content has been decreased exponentially to 9% RH during the electrical heating while the desorption time has been drastically reduced (10 times) from 300 minutes in environmental conditions to 30 minutes when the samples have been electro-activated (Figure 4 a, b). Higher input voltage (15V) leads to a higher desorption rate as well as an increase of moisture loss (7.1 ± 1.3% for 15V and 4.2 ± 0.8% for 10V - Figure 4 a,b). Higher water content at 10V has been observed after actuation and that is due to a lower temperature reached upon the electrical stimulation (Figure 3.b). As a consequence, a slower desorption rate occurs with a pseudo-plateau reached after 30 minutes (Figure 4.b). The desorption rate is close to zero and would lead to a full desorption if the samples were subjected to a higher actuation time.

Within the range of moisture content considered in this work, both the PA6 and the cCF:PA6-I layers undergo some important hygroscopic expansions/shrinkages (ε_z = 2.8% ε_y= 1.1 %) [23] and a significant variation of stiffness (between 20 and 40%) (see supplementary information S2). Nevertheless, the lowest stiffness values observed here are larger than those belonging to the previous hygromorph hydrogel and paper-based actuators. The thermal strain (ε^T) of the active layer is 0.2% for a temperature variation (ΔT) of 21.6°C (Figure 3b), while the hygroscopic strain (ε^h) reaches 2.4% for a moisture content variation (ΔC) of only 7.1%. The hygroscopic strain is 13 times higher than the thermal one in samples subjected to a voltage of 15V. As a consequence, the hygroscopic functionality of the cCF:PA6-I /PA6 bilayers is more important than the thermal capability for the printed multifunctional material.

We have then verified the global electro-thermo-hygroscopic bending actuation of the 4D hygromorph composite materials (Figure 4a and b). The actuation authority shows a similar trend for the two levels of voltage used, with a rapid shape change followed by a stabilization of the curvature. A slight twisting is observed for any voltage due to process-induced defects which prevent the sample symmetry (Figure 4 c,d). With 15V of input, the samples transition from a straight configuration at 98%RH (left in Figure 4a) to a curved one (0.079 ± 0.010 mm^{-1}) similar to those observed in autonomous hygromorph in dry state (0.083 ± 0.017 mm^{-1}). At 10V we could notice a residual curvature δK of 0.021 ± 0.008 mm^{-1} due

to an incomplete desorption (2.87 ± 0.38% after 10V actuation) caused by the lower value of the electrically induced temperature.

These results show the possibility of using voltage to monitor the temperature, the moisture content and therefore the shape change of the material. The relative curvature versus the moisture content (Figure 4.e) during the desorption and subsequent sorption at 98%RH and 23°C after complete drying with the 15V actuation clearly show - again - the full reversibility of the process. A linear fit between change of curvature and moisture content is also observed in this case during both electro-heating and passive sorption (R^2 = 0.99 and R^2=0.96, respectively). The magnitudes of the slopes between electric drying and re-sorption are quite similar (a=0.103 and a=0.107 for electrical drying and re-sorption steps, respectively). This confirms that the passive hygromorph and the active electro-thermo-hygromorph actuations with the present circuit architecture rely on similar actuation principles, although the slope coefficients related to the electro-heating case are one order of magnitude larger than the autonomous one. After one electro-thermo-hygro actuation and a subsequent storage at 98%RH and 23°C the samples recover the shape previously observed during the sorption step (0.093 ± 0.012 mm^{-1}) (Figure 2b). One can therefore assume that no or negligible damage occurs during the electro-heating phase. The 4D printed configuration of the cCF:PA6-I /PA6 hygromorph composite bilayers with the embedded electrical functionality demonstrates therefore the capability of speeding up the desorption of water and the change of shape. The variation of the electric input enables to control the morphing.

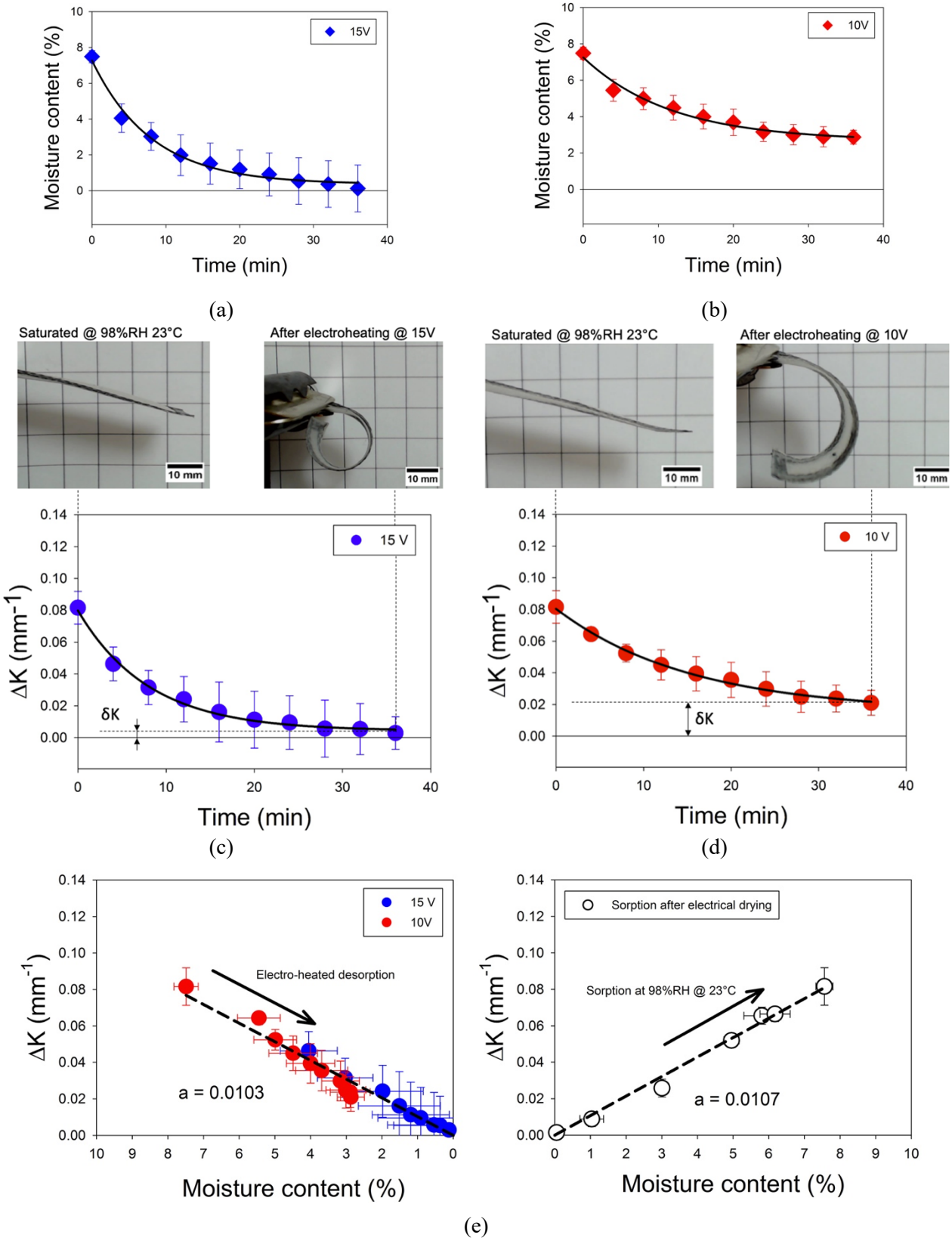

Figure 4: Evolution of the moisture content of the samples saturated at 98%RH and 23°C subjected to 15V (a) and 10V (b). The behaviour fits an exponential decay with $R^2 = 0.993$ and $R^2 = 0.979$ for the 15V and 10V cases. Evolution of the relative curvature electro-thermally activated at 15V (c) and 10V (d) with exponential decay fit ($R^2 = 0.987$ and R^2=0.996 for 15 and 10V, respectively). The coupled pictures show the sample in saturated state at 98%RH and 23°C (left) and after electro-thermally activated desorption (right) at (c) 15V and (d) 10V. (e) The relative curvature versus the moisture content for (left)

both electro-heating actuation, *i.e.* 10 and 15V ($R^2 = 0.99$) and for (right) samples undergoing another sorption step at 98% RH and 23°C after electrical drying ($R^2 = 0.96$).

To underline the potential of this novel class of smart materials made of electro-thermo-hygromorphes over pure passive thermally-actuated morphing structures, similar campaign of tests has been carried out on dried cCF:PA6-I/PA6 bilayers at 9% RH instead that at 98% RH saturated. The initial moisture content in the sample is close to zero to cancel the contribution of the moisture-induced actuation during the electro-thermo-hygromorphing. Once the electrical stimulus is applied (10V or 15V), a rapid change of curvature is observed during the first 60 seconds; this confirms the rapidity of the thermal actuation. The responsiveness (curvature) remains however significantly lower (four times reduced) compared to the electro-thermo-hygromorphing case. This confirms that the novel electro-thermo-hygromorph materials possess a higher degree of hygroexpansion than pure thermal one (Table 1). Once the electrical stimulus is switched-off, the initial curvature is attained with no variation of moisture content.

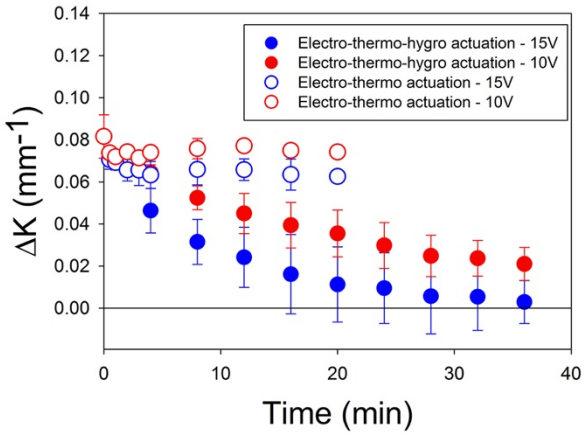

Figure 5: Evolution of the relative curvature of the electro-thermally hygromorphs saturated at 9%RH at 23°C activated at 15V and 10V for initially 98%RH/23°C saturated samples and dried samples. The moisture saturated samples show a higher actuation potential in terms of responsiveness (relative curvature) due to the higher hygroexpansion compared to the pure thermal one.

3. Conclusion

Hygromorphs are class of smart materials continuously developed due to their significant potential for autonomous actuation and large responsiveness. The present work has proposed a novel class of smart multi-stimuli responsive 4D printed hygromorph composite materials that overcome the significant limitations of current hygromorphs (lack on efficient control of the actuation and slow response). This

new class of smart materials also possess load-bearing capabilities and intrinsic control functionalities due to the embedded electro-thermal actuation. The moisture content within the novel materials here presented could vary either autonomously and therefore provide a pure hygromorph actuation, or could be controlled by an electro-thermal stimulus to monitor and control the moisture content, and the resulting curvature. A bilayer microstructure inspired from biological hydraulic actuators like pine cones has been used to optimize the out-of-plane displacement. A commercial printer with conventional material filaments has been used in this work to produce the smart hygromorph materials. Aside from the moisture-sensitive PA6 polymer, we have used cCF:PA6-I composites that can maximize the anisotropy of the resulting hygromorph material.

In this work we have developed hygromorph composites designed using bimetallic-type beam model theory adapted to moisture activation. These materials have shown an autonomous response, with a relatively high bending curvature variation sensitive to the variation of the relative humidity between dry and wet state (98%RH). Another class of active hygromorph materials has been developed based on the use of an electro-thermal stimulus to control the moisture content inside the materials and the curvature. The electrical induced heating of the conductive cCF:PA6-I layer generates a heterogeneous temperature field due to the features of the 4D printing process. The peak temperatures recorded in the samples do not go beyond the glass transition of the cCF:PA6-I and PA-6 layers, and therefore the thermal strains are low. In these materials we can therefore state that the variation of the moisture and the hygroscopic strains dominate the actuation response. When actuated, the multi-stimuli-responsive hygromorph composite materials show a very remarkable 10-fold increase of the actuation speed during desorption compared to the autonomous (passive) hygromorphs samples; the responsiveness of the two classes of materials remains the same. The control of the moisture content with various electrical voltage inputs is evident, and therefore the hygroscopic actuation can be actively triggered and controlled. When the electric current is switched off the hygromorph materials return to be autonomous (passive) actuators, and ambient cooling and moisture drive a fully reversible actuation. When electro-heating is applied to an initially dried sample one can observe the presence of a fast actuation with a very low responsiveness; this further confirms the potential of this novel electro-thermo-hygromorph material as a new and interesting class of smart solids to be used for ambient sensing, but also architected and

deployable structures and mechanical metamaterials by 4D printing with load-bearing capabilities. Moreover, the material reactivity could be further improved through maximizing the hygroscopic expansion gradient between the active and the passive layer in the sample, for instance thanks to the addition of highly moisture sensitive materials such as natural fibres found in hygromorph biocomposites [33]. Additionally, one could also tune the stiffness distribution within the material thanks to 4D printing of anisotropic components (fibrous materials) to develop programmable bioinspired structures [28]. Finally, mechanical instabilities like encountered in biological systems (Dioanea muscipula for instance) could be used in 4D printed structures.

4. Materials and characterization methods

4.1 Sample printing and design

The 3D printer used in this study is a MarkTwo 3D printer provided by Markforged®, which is driven by a web interface (Eiger.io). The filaments, made of multiple strands of carbon fibres coated with PA matrix are also provided by Markforged®. Two spools of filaments are available during the printing, *i.e.* one of neat PA6 filament and one of continuous carbon fibre reinforced PA filament. In the manuscript, one refers to layers printed thanks to continuous carbon fibre reinforced PA filaments as cCF:PA6-I layers. Indeed, the polyamide used in the continuous carbon fibre reinforced filament is identified as a poly hexamethylene isophtalamide (PA6-I) by DSC measurements (not shown here).

Part design is inspired by bilayers biomimetic architectures labelled cCF:PA6-I/PA6. The active and passive layer are made of pure one PA6 layer oriented at +45° and one cCF:PA6-I layer oriented at 90° respectively with a 100% infill. Remaining area within the second layer is filled with PA6 oriented at –45°, 100% infilled.

For each pattern, a degree of freedom has been let to allow binding over actuation. Then, two arms had been designed and electric voltage was applied. Furthermore, two printed configurations have been studied here, *i.e.* the longitudinal and transverse. For each configuration, three different L/W ratios were studied (0.5; 1; 2). Sample width was set to 20 mm and the length of the arms was 30 mm. Finally, layers thickness ratio was theoretically calculated thanks to Timoshenko model [27, 34] by maximizing

theoretical longitudinal curvature variation ΔK. Equations associated to Timoshenko model are shown here.

$$\Delta K = \frac{\Delta\beta\ \Delta C\ f(m,n)}{t} \quad (1)$$

$$f\ (m,n) = \frac{6(1+m)^2}{3(1+m)^2 + (1+mn)\left(m^2 + \frac{1}{mn}\right)} \quad (2)$$

With $m = \frac{t_P}{t_a}$ and $n = \frac{E_P}{E_a}$ where E_P and E_a are the Young's modulus of the wet passive and active layers respectively. $\Delta\beta$ is differential of hygroscopic expansion coefficient between active and passive layers, ΔC is water loss between wet and dry state and t is the total sample thickness. Thus, for longitudinal specimen active thickness t_a is set at 0.375 mm and passive thickness t_P was set at 0.125 mm. For transverse specimen, t_a is set at 0.125 mm and t_p at 0.125 mm with a 100% infill.

4.2 Samples storage

Printed bilayers have been previously dried under vacuum (10 mbar) at 60°C (Vacutherm VT6060 M from Thermo®) until steady weight values were obtained. Then, the bilayers have been stored in chambers with relative humidity (RH) controlled by a saturated solution of potassium hydroxide (KOH), magnesium chloride ($MgCl_2$), sodium chloride (NaCl) and potassium sulphate (K_2SO_4) so as to reach a RH of 10%, 30%, 75% and 98%, respectively. All samples are stored at room temperature (23°C). Samples were used after reaching saturation, i.e. when the weight was stabilized.

4.3 Expansion measurement

Hygroscopic expansion and moisture uptake have been evaluated on printed samples 20 mm (L) x 20 mm (w) x 4 mm (t). Volumetric measurements have been performed with a Mitutoyo micrometer IP65 and gravimetric analyses using a Fischer Scientific PAS214C balance (10^{-4} g). Coefficient of hygroscopic expansion (β) displays as the slope of hygroscopic expansion over moisture content evolution.

Thermal expansion was measured on 10 mm (L) x 10 mm (w) x 10 mm (t) samples thanks to thermomechanical analysis (Q800 DMA) from TA Instruments.

Samples have been placed between two parallel plates and held with a blocking force F = 0,1 N. The samples have been subjected to a 10 K/min temperature ramp from 25°C to 200°C and the thermal expansion ΔL over temperature variation ΔT has been measured thanks to the displacement of one of the parallel plates. The coefficient of thermal expansion α is expressed as equation 3.

$$\alpha = \frac{1}{\Delta T}\frac{\Delta L}{L_0} \tag{3}$$

Where L_0 represents initial sample length. Thus, coefficient of thermal expansion was graphically determined as the slope of the curve $\Delta L/L_0$ against ΔT.

4.4 Hygromorph and electro-thermo-hygro activation

Electric activation has been performed using an Agilant E31610A DC Power Supply generator. Two voltages have been considered (15V and 10V) and a passive drying at 9% RH was carried out in parallel. For each sample the distribution of the thermal field has been observed thanks to a calibrated thermal camera FLIR X6580sc while temperature was measured with a C.A 864 thermometer. Mass variation has been measured thanks to a Fisher Scientific PAS214C balance (10^{-4} g). Curvature variation was tracked thanks to Logitech HD Pro Webcam C920 with 30 frames per second acquisition speed and image treatment was performed thanks to ImageJ 1.51j8 software (National Institutes of Health, USA). Curvature is measured by fitting the evolution of sample shape to a "circle" function. Bending curvature is calculated using the radius of the fitted circle.

4.4 Optical observations

Electrically induced imperfections have been observed thanks to optical microscopy (Leica MZ16 binocular with 16:1 magnification and 840 Lp/mm resolution).

S. Supplementary information

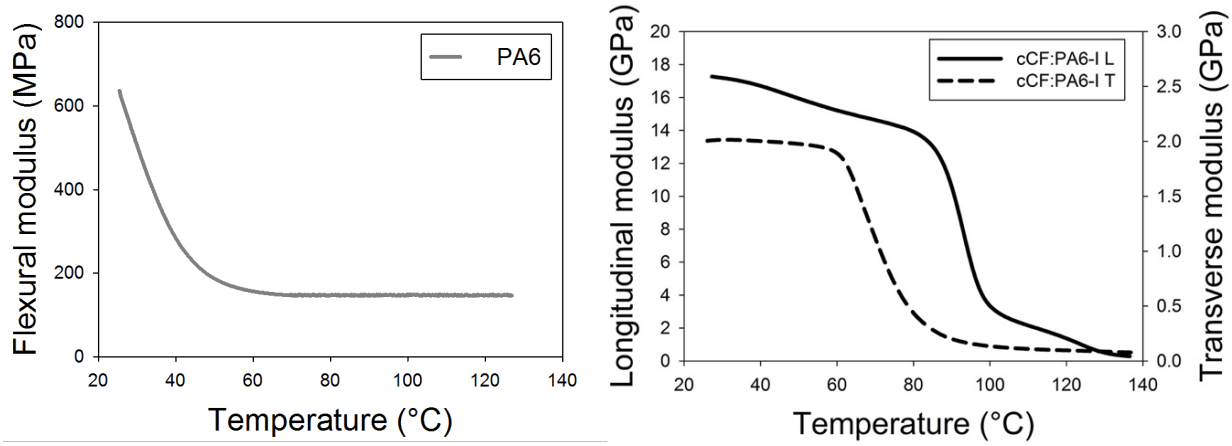

Figure S1 Evolution of (a) the elastic modulus of the PA6, (b) longitudinal and transverse of cCF:PA6-I with temperature.

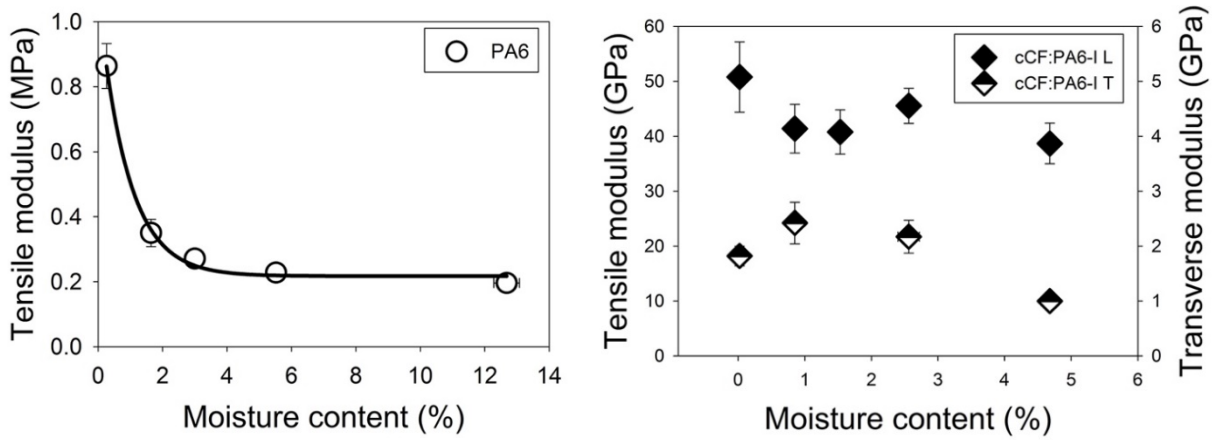

Figure S2 Evolution of (a) the elastic modulus of PA6 , (b) longitudinal and transverse of cCF:PA6-I as a function of the moisture content.

Table S1: Maximal curvature reached for each printed configuration after a storage at 98% RH

Configuration	ΔK (mm^{-1})	
<u>Longitudinal</u>		
L/W = 0.5	0.011 ± 0.002	
L/W = 1	0.012 ± 0.0004	
L/W = 2	0.010 ± 0.002	
<u>Transverse</u>		
L/W = 0.25	0.079 ± 0.010	
L/W = 1	0.052 ± 0.010	
L/W = 2	0.032 ± 0.006	

6. Acknowledgments

The authors wish to acknowledge “Region Bretagne” and CNRS AAP “Biomimetisme” for financial supports. The authors would also like to acknowledge Edouard Geslain, Thomas Pierre, Thibaut Colinart and William Berckman for their contribution regarding the infrared thermography analysis.

7. References

[1] S. Tibbits, 4D printing: multi-material shape change, Archit. Des. (2014) 116–121.

[2] E. Pei, 4D printing – revolution or fad ?, (2015). doi:10.1108/AA-02-2014-014.

[3] Z.X. Khoo, J.E.M. Teoh, Y. Liu, C.K. Chua, S. Yang, J. An, K.F. Leong, W.Y. Yeong, 3D printing of smart materials: A review on recent progresses in 4D printing, Virtual Phys. Prototyp. 10 (2015) 103–122. doi:10.1080/17452759.2015.1097054.

[4] G.N. Levy, R. Schindel, J.P. Kruth, Rapid manufacturing and rapid tooling with layer manufacturing (LM) technologies, state of the art and future perspectives, CIRP Ann. - Manuf. Technol. 52 (2003) 589–609. doi:10.1016/S0007-8506(07)60206-6.

[5] L. Sun, W.M. Huang, Z. Ding, Y. Zhao, C.C. Wang, H. Purnawali, C. Tang, Stimulus-responsive shape memory materials: A review, Mater. Des. 33 (2012) 577–640. doi:10.1016/j.matdes.2011.04.065.

[6] F. Momeni, S. M.Mehdi Hassani.N, X. Liu, J. Ni, A review of 4D printing, Mater. Des. 122 (2017) 42–79. doi:10.1016/j.matdes.2017.02.068.

[7] A.Mitchell, U.Lafont, M.Hołyńska, C.Semprimoschnig, Additive Manufacturing- A Review of 4D Printing and Future Applications, Addit. Manuf. 24 (2018) 606–626.

[8] C. Yang, B. Wang, D. Li, X. Tian, Modelling and characterisation for the responsive performance of CF/PLA and CF/PEEK smart materials fabricated by 4D printing, Virtual Phys. Prototyp. 12 (2017) 69–76. doi:10.1080/17452759.2016.1265992.

[9] L. Ionov, Hydrogel-based actuators : possibilities and limitations, Mater. Today. 17 (2014) 494–503. doi:10.1016/j.mattod.2014.07.002.

[10] A. Sydney Gladman, E.A. Matsumoto, R.G. Nuzzo, L. Mahadevan, J.A. Lewis, Biomimetic 4D printing, Nat. Mater. 15 (2016) 413–418. doi:10.1038/nmat4544.

[11] M.C. Mulakkal, R.S. Trask, V.P. Ting, A.M. Seddon, Responsive cellulose-hydrogel composite ink for 4D printing, Mater. Des. 160 (2018) 108–118. doi:10.1016/j.matdes.2018.09.009.

[12] D. Raviv, Z. Wei, C. McKnelly, A. Papadopoulou, A. Kadambi, B. Shi, S. Hirsch, D. Dikovsky, M. Zyracki, C. Olguin, R. Raskar., S. Tibbits, Active Printed Materials for Complex Self-Evolving Deformations, Sci. Rep. 4 (2014) 1–8.

[13] A. Le Duigou, M. Castro, R. Bevan, N. Martin, 3D printing of wood fibre biocomposites: From mechanical to actuation functionality, Mater. Des. 96 (2016) 106–114. doi:10.1016/j.matdes.2016.02.018.

[14] D. Correa, A. Papadopoulou, C. Guberan, N. Jhaveri, S. Reichert, A. Menges, S. Tibbits, 3D-Printed Wood: Programming Hygroscopic Material Transformations, 3D Print. Addit. Manuf. 2 (2015) 106–116. doi:10.1089/3dp.2015.0022.

[15] M.M. Hamedi, V.E. Campbell, P. Rothemund, F. Güder, D.C. Christodouleas, J.F. Bloch, G.M. Whitesides, Electrically Activated Paper Actuators, Adv. Funct. Mater. 26 (2016) 2446–2453. doi:10.1002/adfm.201505123.

[16] M. Amjadi, M. Sitti, High-Performance Multiresponsive Paper Actuators, ACS Nano. 10 (2016) 10202–10210. doi:10.1021/acsnano.6b05545.

[17] J. Ru, Z. Zhu, Y. Wang, H. Chen, A moisture and electric coupling stimulated ionic polymer-metal composite actuator with controllable deformation behavior, (2018).

[18] L. Ionov, Biomimetic hydrogel-based actuating systems, Adv. Funct. Mater. 23 (2013) 4555–

4570. doi:10.1002/adfm.201203692.

[19] W. Liu, H. Chen, M. Ge, Q.Q. Ni, Q. Gao, Electroactive shape memory composites with TiO2whiskers for switching an electrical circuit, Mater. Des. 143 (2018) 196–203. doi:10.1016/j.matdes.2018.02.005.

[20] L. Chen, M. Weng, F. Huang, W. Zhang, Light- and humidity-driven actuators with programmable complex shape- deformations, Sensors Actuators B. Chem. 282 (2019) 384–390. doi:10.1016/j.snb.2018.11.067.

[21] L. Chen, M. Weng, P. Zhou, L. Zhang, Z. Huang, W. Zhang, Multi-responsive actuators based on a graphene oxide composite: intelligent robot and bioinspired applications, Nanoscale. (2017).

[22] Y. Mao, Z. Ding, C. Yuan, S. Ai, M. Isakov, J. Wu, T. Wang, M.L. Dunn, H.J. Qi, 3D Printed Reversible Shape Changing Components with Stimuli Responsive Materials, Sci. Rep. 6 (2016) 1–13. doi:10.1038/srep24761.

[23] G. Chabaud, M. Castro, C. Denoual, A. Le Duigou, Hygromechanical properties of 3D printed continuous carbon and glass fibre reinforced polyamide composite for outdoor structural applications, Addit. Manuf. 26 (2019) 94–105.

[24] G. Wypych, Handbook of polymers (Second edition), Second, ChemTec Publishing, 2016. doi:10.1016/B978-1-895198-92-8.50002-1.

[25] A. Le Duigou, M. Castro, Evaluation of force generation mechanisms in natural, passive hydraulic actuators, Sci. Rep. 6 (2016). doi:10.1038/srep18105.

[26] S. Poppinga, C. Zollfrank, O. Prucker, J. Rühe, A. Menges, T. Cheng, T. Speck, Toward a New Generation of Smart Biomimetic Actuators for Architecture, Adv. Mater. 1703653 (2017) 1703653. doi:10.1002/adma.201703653.

[27] S. Timoshenko, Analysis of bi-metal thermostats, J. Opt. Soc. Am. 11 (1925) 233–255.

[28] R.M. Erb, J.S. Sander, R. Grisch, A.R. Studart, Self-shaping composites with programmable bioinspired microstructures ´, Nature. (2013) 1–8. doi:10.1038/ncomms2666.

[29] J.M. Skotheim, L. Mahadevan, Physical Limits and Design Principles for Plant and Fungal Movements, Science (80-.). 308 (2005) 1308–1310. doi:10.1126/science.1107976.

[30] L. Lim, I.A.N.J. Britt, M.A. Tung, Sorption and Transport of Water Vapor in Nylon 6 , 6 Film, J. Appl. Polym. Sci. 71 (1998) 197–206.

[31] Q. Wang, X. Tian, L. Huang, D. Li, A. V. Malakhov, A.N. Polilov, Programmable morphing composites with embedded continuous fibers by 4D printing, Mater. Des. 155 (2018) 404–413. doi:10.1016/j.matdes.2018.06.027.

[32] A. Le Duigou, M. Castro, Hygromorph BioComposites: Effect of fibre content and interfacial strength on the actuation performances, Ind. Crops Prod. 99 (2017) 142–149. doi:10.1016/j.indcrop.2017.02.004.

[33] A. Le Duigou, S. Requile, J. Beaugrand, F. Scarpa, M. Castro, Natural fibres actuators for smart bio-inspired hygromorph biocomposites, Smart Mater. Struct. 26 (2017). doi:10.1088/1361-665X/aa9410.

[34] E. Reyssat, L. Mahadevan, Hygromorph: from pine cone to biomimetic bilayers, J. R. Soc. 6 (2009) 951–957.

[35] N.L. Hancox, The compression strength of unidirectional carbon fibre reinforced plastic, J. Mater. Sci. 10 (1975) 234–242. doi:10.1007/BF00540347.

[36] P.Z. J.A. Nairn, Matrix solidification and the resulting residual thermal stresses in composites, J Mater Sci. 20 (1985) 355–367.